Regional cardiac tissue oxygenation as a function of blood flow and pO$_2$: a near-infrared spectroscopic imaging study

Stephen P. Nighswander-Rempel
Valery V. Kupriyanov
R. Anthony Shaw
National Research Council of Canada
Institute for Biodiagnostics
435 Ellice Avenue, Winnipeg
Manitoba R3B 1Y6, Canada

Abstract. Near-infrared spectroscopic imaging (NIRSI) is useful to assess cardiac tissue oxygenation in arrested and beating hearts, and it shows potential as an intraoperative gauge of the effectiveness of bypass grafting. The purpose of this study was to determine whether NIRSI can reliably differentiate among a range of cardiac oxygenation states, using ischemia and hypoxia models independently. An ischemia-reperfusion model was applied to isolated, beating, blood-perfused porcine hearts, in which the left anterior descending (LAD) artery was cannulated. LAD flow was decreased stepwise to approximately 50, 20, and 0% of normal flow and was completely restored between ischemic episodes. Upon completion of the ischemia-reperfusion protocol, the hearts were further subjected to periods of increasingly severe global hypoxia. Regional oxy- and deoxyhemoglobin (myoglobin) levels were derived from spectroscopic images (650 to 1050 nm) acquired at each step. Oxygenation maps vividly highlighted the area at risk for all degrees of ischemia. Oxygenation values differed significantly for different LAD flow rates, regardless of whether intermediate reperfusion was applied, and oxygenation values during progressive hypoxia correlated well with blood oxygen saturation. These results suggest that NIRSI is well suited, not only to identify ischemic or hypoxic regions of cardiac tissue, but also to assess the severity of deoxygenation. © *2006 Society of Photo-Optical Instrumentation Engineers.* [DOI: 10.1117/1.2357601]

Keywords: ischemia; hypoxia; hemoglobin; near-infrared; spectroscopy; imaging.

Paper 04211RRRR received Nov. 5, 2004; revised manuscript received Jul. 22, 2005 and May 11, 2006; accepted for publication Jun. 6, 2006; published online Oct. 9, 2006.

1 Introduction

Coronary artery disease (CAD) is a leading cause of mortality in developed countries. Bypass operations have become increasingly common in treating CAD, raising a need for intraoperative imaging modalities to aid in assessing the effectiveness of the surgical intervention. While various techniques are available to monitor coronary perfusion and cardiac function noninvasively, including radionuclide methods, computed tomography, and magnetic resonance imaging,[1–3] they are impractical for use during open-heart surgery because of equipment size and cost. Echocardiography and x-ray angiography have also been applied to monitor coronary arterial flow,[4,5] but neither technique provides any information regarding the adequacy of blood and tissue oxygenation (which depends on the oxygen supply-demand ratio).

Both visible and near-infrared spectroscopy have been exploited to characterize tissue oxygenation, typically employing fiber optic bundles to illuminate the tissue and to gather reflected light and transmit it to a spectrometer.[6–30] Hemoglobin (Hb) and myoglobin (Mb) both contribute substantially to the visible and near-infrared spectra, and the spectra are very similar for the two species. While there are reports that the contributions of Mb and Hb can be resolved in blood-perfused tissues,[11,25–30] many investigations of cardiac tissue have made use of Hb-free perfusate to permit characterization of Mb oxygenation.[6–17] These experiments are carried out with isolated working hearts. Experiments with blood-perfused hearts both on perfusion circuits[26,29] and *in situ* for both animals[18–23,28] and human cardiac arterial bypass graft patients[24] have demonstrated changes in myocardial oxygenation in response to physical or pharmacological manipulations.

By their nature, fiber optic near-infrared spectroscopic measurements do not easily reveal spatial variations in oxygenation. Optical imaging methods have therefore been developed previously and applied to cardiac tissue, exploiting both intrinsic reduced nicotinamide adenine dinucleotide (NADH) fluorescence[31–43] and the phosphorescence of extrinsic probes that are quenched by dissolved oxygen.[43,44] To complement

Address all correspondence to R. Anthony Shaw, National Research Council of Canada, Institute for Biodiagnostics, 435 Ellice Avenue, Winnipeg, Manitoba R3B 1Y6 Canada; Tel: 204-984-4626; Fax: 204-984-5472; E-mail: anthony.shaw@nrc-cnrc.gc.ca

these techniques, we have recently introduced near-infrared spectroscopic imaging (NIRSI) as a means to map regional oxygenation in both arrested and beating hearts.[45–48] This approach combines the sensitivity of near-infrared spectroscopy to changes in tissue oxygenation with the spatial resolution available with imaging, capitalizing on the relatively deep penetration of near-infrared light (650 to 1200 nm) into tissue (>5 mm) as compared to visible light (<5 mm). The advantages of this technique include its low cost, ease of transport, lack of physical contact with the tissue under study, and excellent spatial resolution. All of these make it well-suited for potential use in an intraoperative setting.

As a direct probe of heme oxygenation status, NIRSI is well-suited to measure regional variations in cardiac blood (tissue) oxygenation—a feature that is shared by the fluorescence photography (imaging) technique introduced three decades ago by Barlow and Chance.[31] While NIRSI exploits optical transitions of oxy- and deoxy-hemoglobin (myoglobin), the fluorescence images reveal the distribution of the reduced NADH component of the NADH-NAD couple. NADH fluorescence is in turn an indicator of intracellular oxygen concentration in Langendorff-perfused cardiac tissue (Hb absorptions preclude the use of this technique in blood-perfused hearts). Apart from the difference between the chromophores by which oxygenation is revealed, the key features distinguishing the two imaging modalities are spatial resolution and penetration depth. The majority of published cardiac fluorescence imaging studies have used film as the imaging sensor, which by its nature confers better resolution than a 256×256–charge-coupled device (CCD) array sensor for a given field of view. On the other hand, NIRSI offers deeper tissue penetration, probing to a depth of several millimeters as compared to ~ 100 μm for NADH fluorescence imaging. The techniques are complementary in that sense, with fluorescence imaging offering a relatively clear and detailed view of epicardial oxygen distribution, and NIRSI probing more deeply to sample subepicardial and midmural tissues.

The present study reports near-infrared spectroscopic images of isolated beating pig hearts with Langendorff perfusion using a 50:50 Krebs-Henseleit buffer-blood mixture. These experiments were designed to achieve two specific objectives. First, while a previous study correlated the severity of regional ischemia with the severity of regional deoxygenation (as revealed by NIRSI oxygenation maps), it was not clear whether the poor oxygenation was due solely to the severity of the ischemia or whether the duration of the ischemic episode also played a role.[46] This study disentangles those two effects by including intermediate reperfusion between episodes of partial and total regional ischemia. Second, the physical significance of the numerical oxygenation values and related parameters provided by NIRSI maps is not well-understood. To seek relevant insights, we have correlated spectroscopically determined oxygenation values with measured blood oxygen saturation data during periods of increasingly severe global cardiac hypoxia.

2 Materials and Methods

A regional ischemia protocol was carried out using isolated pig hearts, chosen because of their close similarity to human hearts. The animals were treated in accordance with the "Guide to the Care and Use of Experimental Animals" published by the Canadian Council on Animal Care (2nd ed., Ottawa, Ontario, 1993).

2.1 Surgical Procedure

Domestic pigs weighing 32.0±6.5 kg (n=4) were conditioned for 10 days to minimize transport stress. General anesthesia and surgery were performed as described previously.[49] Cardiac arrest was induced by injection of 300 to 400 ml of cold, cardioplegic Krebs-Henseleit buffer (KHB) containing 21 mM K^+ through the right carotid artery. Normal KHB contained 25 mM $NaHCO_3$, 118 mM NaCl, 1.2 mM KH_2PO_4, 3.5 mM KCl, 1.75 mM $CaCl_2$, 1.2 mM $MgSO_4$, 0.5 mM Ethylenediaminetetraacetic acid (EDTA)-2Na, 11.0 mM glucose, and 6 g/L albumin. The isolated heart was placed in cold, cardioplegic KHB and then cleaned, and a drain was placed in the left ventricle. Over 1 L of blood (mixed with high-potassium KHB) was collected for perfusion during the experiment. A catheter was inserted into the subclavian artery to provide a connection to the perfusion (aortic) pressure line. The left atrium was opened and a latex balloon was inserted into the left ventricle, positioned, secured, and connected to a pressure transducer [Gould P23Db (Gould Inc., Cleveland, Ohio)]. A catheter was placed in the coronary sinus to collect venous effluent samples and a perfusion cannula was secured in the aorta via the brachiocephalic artery. A cannula ($\sim$2-mm i.d.) connected to a three-way stopcock through a piece of silicon tubing was filled with saline and then inserted through the incision into the LAD approximately 10 mm below the circumflex artery and secured in place. The depth of penetration of the cannula into the artery was minimal (typically $\sim$2 mm) to avoid obstruction of small branches arising from the LAD.

2.2 Heart Perfusion

The whole blood containing elevated K^+ levels was mixed with 1 L of KHB (36°C) to which no KCl had been added ($[K^+]$=1.2 mM) in order to restore $[K^+]$ to normal levels. Hearts (197±52 g) were perfused by the Langendorff method with this solution (2.5 to 3.5 L circulation volume). Prior to perfusion, the K^+ level of the perfusate was measured and, if the potassium concentration was low, KCl was added to the perfusate to maintain a mean K^+ concentration of 4.6±0.2 mM (Table 1). At the beginning of perfusion, the perfusate contained 8.4±1.2 mM glucose, 2.0±0.1 mM lactate, 51±10 g/L Hb ($\sim$50% of normal content in pig blood), heparin (10 000 units per liter), and 1 μM propranolol (beta-blocker). Propranolol was used to neutralize the effects of endogenous catecholamines in blood and bring the heart rate (HR) to normal levels [103±20 beats per minute (bpm)] that are convenient for image gating. The perfusate was aerated in a membrane oxygenator (Cobe, Japan) with a 95% O_2/5% CO_2 gas mixture (pO_2=546±35 mm Hg) and supplied to the heart at a constant flow of approximately 1.5 ml/min/g wet weight.

Left ventricular systolic pressure [(LVSP), 81±16 mm Hg], end-diastolic pressure [(LVEDP), 4.3±2.5 mm Hg], and HR were monitored. Perfusion pressure (55±7 mm Hg at the baseline) was measured through tubing connected to the aortic line. Cardiac performance was

Table 1 Concentrations of some blood components during experimental protocol.

Step	K$^+$ (mM/L)	Glucose (mM/L)	Lactate (mM/L)	Hb (g/L)
1. Baseline	4.6±0.2	8.4±1.2	2.0±0.1	51±10
2. 50% flow	4.6±0.3	8.1±1.1	2.0±0.2	52±9
p versus 1	NS	0.02	NS	NS
3. Reperfusion	4.7±0.3	8.1±0.9	2.0±0.4	53±10
p versus 1	NS	NS	NS	NS
4. 20% flow	4.8±0.2	7.7±0.8	2.3±0.3	53±10
p versus 1	0.007	0.03	NS	NS
5. Reperfusion	4.7±0.2	7.6±0.8	2.5±0.4	53±9
p versus 1	NS	0.03	0.04	NS
6. No flow	4.8±0.2	7.3±0.8	2.7±0.5	53±8
p versus 1	0.04	0.01	0.03	NS
7. Reperfusion	4.8±0.3	7.1±0.8	3.2±0.6	54±10
p versus 1	NS	0.01	0.02	NS

Means ± standard deviations for hearts are shown. Data correspond to end of each protocol step. *P* values for comparisons with baseline parameters were calculated using paired Student's *t*-test (NS=not significant).

determined as a pressure-rate product $[PRP=HR \times (LVSP-LVEDP), 7600 \pm 1530$ mm Hg/min$]$. The balloon volume was adjusted to bring LVEDP to 0 to 7 mm Hg and LVSP to 63 to 98 mm Hg at a HR of 88 to 129 bpm. The left anterior descending (LAD) artery was cannulated and the cannula was connected to a branch of the perfusion line filled with perfusate and equipped with a bubble trap, variable clamp, and flowmeter probe (Transonic Systems, Inc., Ithaca, New York). This branch was connected to a BSD Advanced Heat Exchanger (Sorin Biomedical Inc., California) that served as a bubble trap for the major (aortic) perfusion line and as an additional heat exchanger. At the beginning of perfusion, the LAD line was fully open providing adequate flow (40 to 45 ml/min) through the LAD bed. To induce regional ischemia, the clamp was completely or partially closed to provide zero flow (collateral flow only) or flow reduced to 20 or 50% of the baseline.

Glucose, lactate, pO$_2$, pCO$_2$, pH, Na$^+$, K$^+$, Ca^{2+}, and Cl$^-$ were monitored in arterial and venous samples using a Stat Profile CCX 9 analyzer (Nova Biomedical, Waltham, Massachusetts). Hb and its oxygen saturation were measured immediately after sampling, using an OSM3 hemoxymeter analyzer (Radiometer, Copenhagen). Arterial pO$_2$ was maintained at 435 to 597 mm Hg and arterial pH was in the range of 7.35 to 7.45. The oxygen consumption rate $[V(O_2)]$ was calculated as a product of arterio-venous $[O_2]$ difference and total coronary flow divided by heart mass (μmol/min/g) due to complete Hb saturation with O$_2$ in venous blood. Electrocardio-

gram (ECG) wires were attached to the heart to monitor the cardiac cycle.

2.3 Image Acquisition and Analysis

Images were acquired as described previously[45,46] with an infrared-sensitive, back-illuminated 256×256-pixel CCD-array camera (Photometrics, Tucson, Arizona). With the lens and measurement geometry employed here, each pixel corresponded to an area of approximately 0.4×0.4 mm on the heart surface. A liquid crystal tuneable filter [(LCTF), Cambridge Research and Instrumentation, Woburn, Massachusetts] with an adjustable bandpass and a 10-nm bandwidth was mounted to the camera lens. Images were acquired at 10-nm wavelength intervals between 650 and 1050 nm, providing a complete absorbance spectrum for each pixel. Wavelength selection was controlled by LABVIEW software (National Instruments, Austin, Texas).

The isolated, perfused, beating hearts were illuminated with quartz halogen floodlights and raw reflectance cardiac image sequences were acquired. The lamps were placed at an oblique angle, relative to the line of sight with the camera, to minimize specular reflection. Image acquisition was triggered by the peak of the QRS complex of the ECG and a delay was set at between 350 and 500 ms to reduce motion artifacts by ensuring that all images were acquired during diastole. Since absorptivity spectra of Hb and Mb are nearly identical, the spectral features exhibited here reflect absorption by both species, designated here as oxy-(Hb+Mb) and deoxy-(Hb+Mb). Acquired spectra were fitted with these absorptivity spectra to determine relative oxy-(Hb+Mb) and deoxy-(Hb+Mb) concentration values.[45,46] This technique models the spectra as weighted sums of the constituent absorptivity spectra (oxy-Hb+Mb, deoxy-Hb+Mb, water, and a baseline offset term) and applies a linear regression to calculate the constituent concentrations. The optimal least-squares fit minimizes the spectral residual over the spectral range of 650 to 890 nm (Fig. 2). Oxygenation values were then calculated as the ratio of oxy-(Hb+Mb) to total-(Hb+Mb).

2.4 Experimental Protocol

Each heart underwent a stepwise graded regional ischemia protocol with 15-min periods of reperfusion following each 15-min period of graded ischemia (to minimize irreversible ischemic damage that may arise with prolonged uninterrupted ischemia, Fig. 1). Previous work by our group has indicated that a 15-min reperfusion is sufficient to restore oxygenation to normal levels following partial ischemia.[47] Following an equilibration period of 30 to 40 min, LAD flow to the area at risk (21±2% of the left ventricular mass) was reduced from 40±7 ml/min to half of the equilibrium value (18±2 ml/min) and then restored (40±9 ml/min). LAD flow was reduced further to 20% of equilibrium levels (6.3±1.3 ml/min) and again restored (44±7 ml/min). LAD flow was then stopped completely, followed by another period of reperfusion (45±7 ml/min). Spectroscopic images were acquired for the anterior side of the heart at each step.

Graded hypoxia experiments followed the intermittent ischemia protocol. These experiments served as the basis to correlate oxygenation readings derived spectroscopically (both for bulk tissue and for regions localized on surface ar-
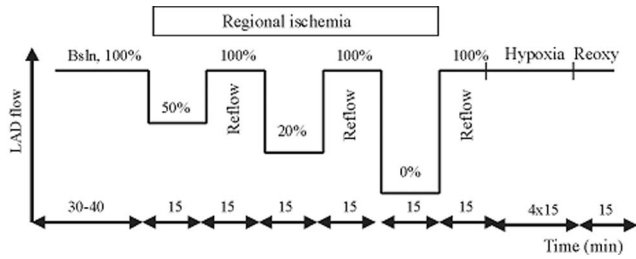
Fig. 1 Experimental protocol. After 30 min of equilibration with normal perfusion, LAD flow is reduced to 50, 20, and 0% for 15 min each. After each period of regional ischemia, the LAD bed is reperfused. Following completion of the regional ischemia procedure, four periods of progressively increasing hypoxia at normal flow are applied (see Sec. 2.4).

teries) with the actual arterial and venous oxygenation as determined by oxymetry of blood samples (the actual arterial and venous blood oxygenation within the ischemic area is unknown). The hearts were subjected to four 15-min periods of increasing hypoxia at constant flow (48.5 ± 9.3 ml/min), by replacing O_2 with N_2 in the gas mixture (95% O_2/5% CO_2+95% N_2/5% CO_2) such that O_2 decreased from 95 to nearly 0%. As a consequence, arterial (and venous) O_2 saturation of Hb was reduced stepwise from 100% ($98 \pm 1\%$) to $36 \pm 6\%$ ($17 \pm 6\%$), followed by restoration of oxygenation to 100%. Blood samples were taken and spectroscopic images were acquired after at least 10 min of hypoxia at each stage. Four 15-min periods of hypoxia did not significantly affect the PRP value, which was $42 \pm 10\%$ of baseline immediately before hypoxia and $36 \pm 6\%$ following hypoxia.

During the ischemia-reperfusion protocol, glucose decreased by 1.3 mM and lactate increased by 1.2 mM, indicating that glucose oxidation and anaerobic glycolysis both con-
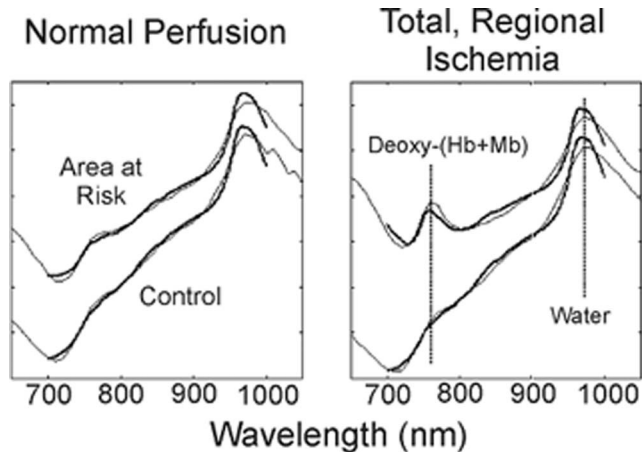
Table 2 Changes in cardiac function and oxygen uptake in pig hearts induced by changes in LAD flow.

Step	HR (bpm)	LVSP (mm Hg)	PRP (mm Hg/min)	V(O$_2$) (μmol/min/g)
1. Baseline	103 ± 20	81 ± 16	7998 ± 1777	0.83 ± 0.14
2. 50% flow	102 ± 21	59 ± 17	5428 ± 1706	0.75 ± 0.07
p value	NS	0.002	0.001	NS
3. Reperfusion	99 ± 23	70 ± 21	6930 ± 2497	0.78 ± 0.05
p value	NS	NS	NS	NS
4. 20% flow	101 ± 22	34 ± 11	2713 ± 699	0.75 ± 0.06
p value	NS	0.001	0.003	NS
5. Reperfusion	103 ± 22	55 ± 9	4958 ± 952	0.87 ± 0.18
p value	NS	0.005	0.01	NS
6. No flow	106 ± 20	21 ± 4	1465 ± 795	0.70 ± 0.12
p value	NS	0.002	0.003	0.02
7. Reperfusion	99 ± 12	45 ± 7	3688 ± 901	0.82 ± 0.20
p value	NS	0.003	0.006	NS

Means ± standard deviations for hearts are shown. Data correspond to end of each protocol step. P values for comparisons with baseline parameters were calculated using paired Student's t-test (NS=not significant).

tributed to glucose consumption. The subsequent periods of hypoxia and reoxygenation further reduced glucose by 0.9 mM and increased lactate by 1.4 mM (Table 1); these changes were due primarily to anaerobic glycolysis. The HR remained constant throughout the ischemia-reperfusion protocol, but systolic pressure decreased to 56 to 60% of the baseline and PRP to 46 to 58% (Table 2). Subsequent hypoxic periods decreased the PRP slightly from 46 to 36% of the baseline. The oxygen consumption rate did not change.

2.5 Statistical Methods

All statistical tests for significance were performed using the paired, one-tailed Student's t-test. Differences were deemed to be significant if the resulting p value was below 0.05.

3 Results

3.1 Graded Regional Ischemia

This study sought to validate the ability of NIRSI to discriminate among varying degrees of partial ischemia. To that end, oxygenation maps corresponding to each stage of the protocol are displayed in Fig. 3. There is a marked decrease in oxygenation within the LAD perfusion bed (area at risk) during 50% LAD flow as compared to normal perfusion, and this is most noticeable in the arterial branches of the LAD. When LAD flow was further reduced to 20% of normal levels, tissue oxygenation in the affected region also decreased significantly as compared to 50% flow. Stopping LAD flow completely caused tissue oxygenation to fall even further. While reperfu-

Fig. 2 Sample spectra for the area at risk (top) and control tissue (bottom) during normal perfusion and regional ischemia in isolated pig hearts. Note: the spectra are offset for clarity of presentation. Measured spectra are shown in light gray, and reconstructed spectra based on spectroscopically derived deoxy-(Hb+Mb), oxy-(Hb+Mb), and water levels are shown in bold. The absorbance maxima of deoxy-(Hb+Mb) and water at 760 and 975 nm, respectively, are evident. The absorbance band of oxy-(Hb+Mb) centred at 920 nm is very broad and thus not resolved visually from the other bands in the experimental spectra.

sion between ischemic periods consistently restored oxygenation to levels at or slightly above those of baseline perfusion, the decreases in tissue oxygenation (resulting from increased severity of ischemia) were consistent with the trends reported previously for stepwise ischemia without intermittent reperfusion.[47] This observation suggests that the degree of deoxygenation is related only to the severity of ischemia, and not to the duration of preceding ischemic episodes.

To characterize the changes in oxygenation in response to changes in flow, two regions of interest (ROIs) were defined for each heart. One corresponded to left ventricular tissue affected by LAD occlusion (area at risk) and the second to tissue perfused normally throughout the regional ischemia (control). Plots of mean oxygenation through the course of the protocol within each ROI confirmed that the decreases in oxygenation (with increased severity of ischemia) observed in Fig. 3 are consistent and statistically significant [Fig. 4(a)]. Previous work has shown baseline Mb oxygen saturation in blood-perfused guinea pig hearts to be 93%.[29] This is in exact agreement with our values for (Hb+Mb) oxygenation in control tissue. The fact that oxygenation within the area at risk was marginally lower in the area at risk during normal perfusion suggests that the mere placement of the cannula into the LAD hindered flow to some extent and hence reduced oxygenation. Indeed, LAD flow per gram of tissue was slightly lower than that for the entire heart (1.24 ± 0.43 versus 1.44 ± 0.25 ml/min/g). The fact that such small variations in flow produced consequences detectable with NIRSI demonstrates the sensitivity of this technique.

In addition to charting the severity of oxygenation within an area at risk, it is also instructive to monitor the size of the ischemic region throughout the protocol. To that end, the fractional area of cardiac tissue (within the field of view) for which oxygenation fell as compared to normal perfusion was determined for each time point [Fig. 4(b)] and characterized as mild (<10% change), moderate (10 to 20% change), or severe (>20% change). Interestingly, the total area affected by the occlusion (sum of mild, moderate, and severely deoxygenated areas) remained constant at 70% of heart tissue within the field of view even as LAD flow was reduced to 50, 20, and 0% of normal values. Only the severity of deoxygenation was affected. As LAD flow was reduced, the area exhibiting moderate deoxygenation rose from 15% of tissue (at 50% flow) to 28% (20% flow) and 21% (0% flow). The fraction of severely deoxygenated tissue increased from 3% (50% flow) to 11% (20% flow) and further to 24% (0% flow). These results indicate that the main feature distinguishing partial from complete regional ischemia is not the regional extent of tissue affected, but rather the extent to which that area becomes deoxygenated.

3.2 Graded Global Hypoxia

Following the ischemia protocol, hearts were subjected to increasingly severe periods of global hypoxia. Spectroscopic images acquired during stepwise global hypoxia vividly demonstrate the widespread reduction in oxygenation with each increase in the severity of hypoxia (Fig. 5); indeed, the oxygenation exhibited during severe hypoxia is comparable to that exhibited during total, regional ischemia. It is interesting to observe that while mild periods of hypoxia caused substan-
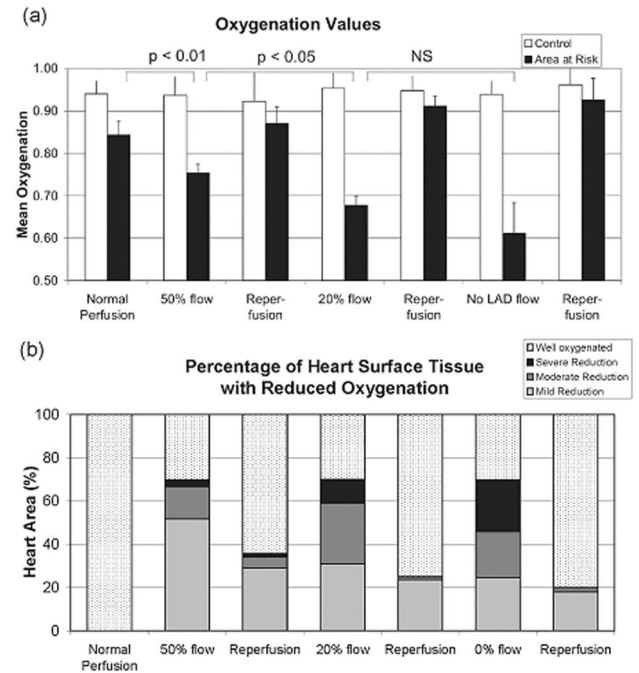

Fig. 4 (a) Mean oxygenation values for control tissue and the area at risk for each step of the experimental protocol. *P* values denote the significance of changes in the area at risk between successive time periods corresponding to 50, 20, and 0% flow. (b) Percentage of heart tissue within the field of view exhibiting oxygenation mildly (<10%, light gray), moderately (10 to 20%, dark gray), or severely (>20%, black) below normal levels. Proportions of tissue with oxygenation at or above normal levels are also shown (dots).

tial reductions in arterial oxygenation, the corresponding reductions in tissue oxygenation were relatively modest. This may reflect the O_2 buffering capacity of Mb, which may remain well-oxygenated despite the large decrease in blood oxygenation.

To explore the quantitative relationship between spectroscopically derived blood and tissue oxygenation values and corresponding measured blood oxygen saturation values, two ROIs were defined. One was restricted to the LAD artery, with the rationale that spectra within this region should reflect arterial Hb oxygenation (with little contribution from Mb). A second ROI encompassed bulk tissue well removed from the major arteries, with the expectation that spectra within this region should broadly reflect both Hb and Mb oxygenation. Mean (spectroscopically derived) oxygenation values were then evaluated separately for each of the two (arterial and tissue) ROIs for correlation with oxygen saturation measured for arterial and venous blood samples.

Oxygenation values derived spectroscopically for the LAD arterial ROI correlated well with measured arterial blood oxygen saturation values [$R^2=0.937$, slope=0.72; see Fig. 6(a)]. However, since the spectroscopic data represented the oxygenation of a region corresponding to a major artery and hence excluded the contributions of Mb (or venous blood), extrapolation of this relationship to tissue regions may be unreliable.

A second analysis correlated the oxygenation values derived for bulk tissue regions remote from major arteries to the
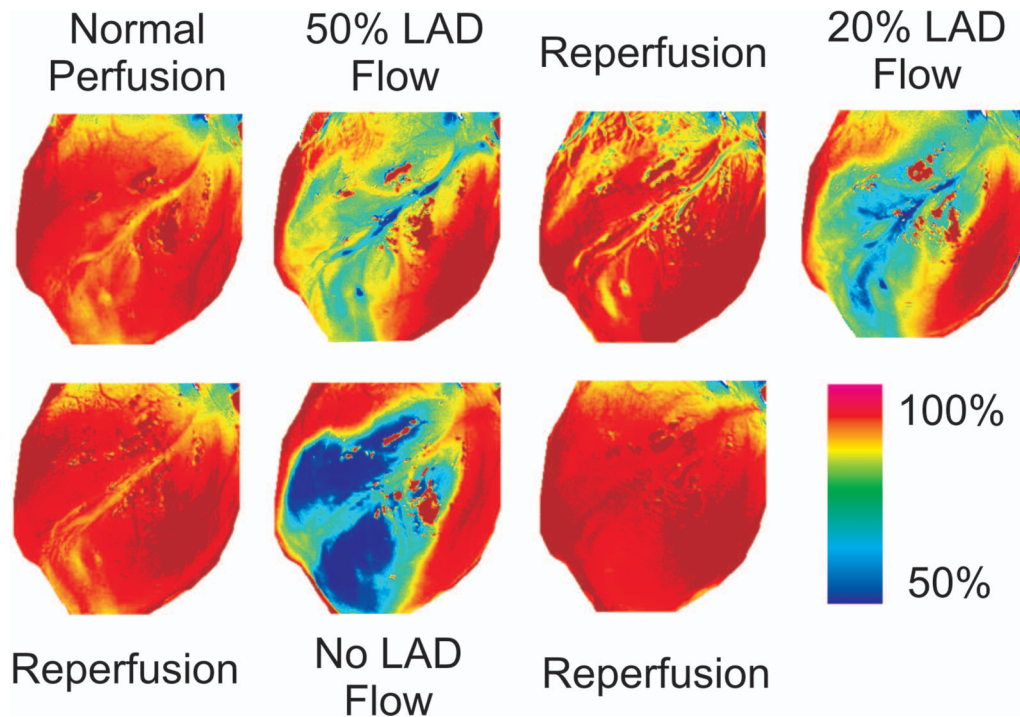
Fig. 3 Changes in oxygenation parameters during periods of ischemia and reperfusion. The color of each pixel on the anterior side of the heart indicates the value of the oxy-(Hb+Mb) to total (Hb+Mb) ratio. Well-oxygenated areas are shown in red, while poorly oxygenated areas are shown in blue.
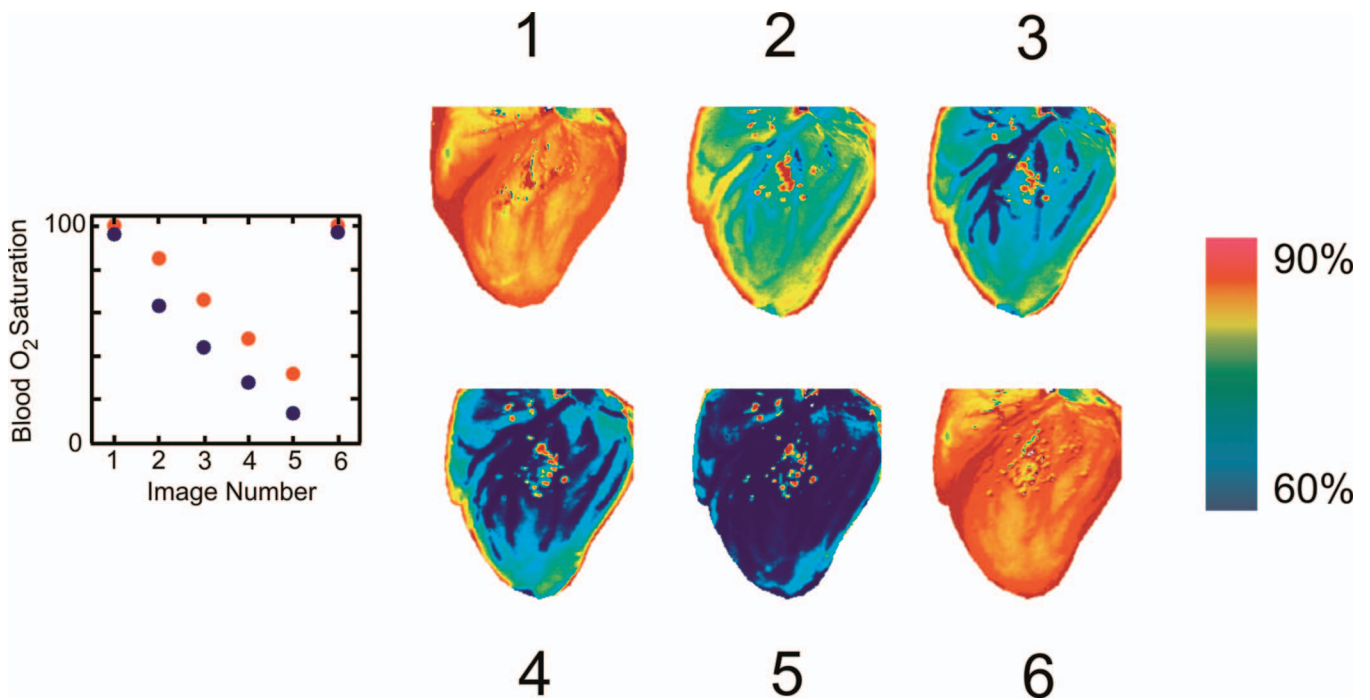

Fig. 5 Cardiac oxygenation maps during periods of increasingly severe global hypoxia. On the far left is a plot depicting arterial (red) and venous (blue) oxygen saturation values at each corresponding time point.

mean (arterial and venous) blood oxygen saturation values. These data also exhibited a close linear relationship [Fig. 6(b)], although the slope (0.40, $R^2 = 0.926$) deviated much more significantly from unity. The low slope likely originates in part from spectral contributions of Mb, since Mb is more completely saturated at low oxygen pressures than Hb. Thus, for a given blood oxygen level, spectroscopically derived tissue oxygenation values were higher for bulk cardiac tissue than for the LAD artery [cf. ordinate values in Figs. 6(a) and 6(b)].

4 Discussion

4.1 What Does NIRSI Measure in Cardiac Tissue?

The oxygenation parameter used in this study, oxy-(Hb+Mb)/total-(Hb+Mb) reflects spectroscopic contributions from both Hb and Mb. The prominence of oxy- and deoxy-Hb absorptions for cardiac tissue depend upon the tissue Hb content, which is in turn proportional to the capillary blood volume (about 8% in pig hearts under normal conditions).[11] Under conditions identical to those used here, Mb has been previously estimated to provide nearly two-thirds of the total heme absorption in cardiac tissue.[48] During graded hypoxia, when coronary flow and perfusion pressure both remain stable, blood volume and the total-Hb fraction should be constant. Under these conditions, a good linear correlation was observed between arterial Hb oxygen saturation and oxygenation as determined by NIRSI [Fig. 6(a)]. In contrast, during graded ischemia, when the LAD flow and pressure decreased gradually to near-zero values, blood volume (and hence the total-Hb fraction) would be expected to decrease significantly. Therefore, the relative contribution of Mb to the spectra should increase (with the obvious exception of large, surface blood vessels such as the LAD, where the Hb contribution continues to dominate the signal). This may partially explain the high oxygenation values exhibited during complete ischemia, as Mb may remain oxygenated while Hb becomes deoxygenated.

Separate determination of Hb and Mb oxygenation is complicated by a variety of factors. First, Hb and Mb are exposed to very different O_2 concentrations even under normal physiological conditions (60 to 500 and 6 to 8 μM, respectively) and have different dissociation constants for O_2 (25 and 2.5 μM).[13,50] Furthermore, the oxygen saturation curves for Hb and Mb differ significantly: that of Hb is sigmoidal due to cooperativity between the four subunits, whereas that of Mb is hyperbolic. Therefore, while Hb and Mb are nearly fully saturated under normal conditions, their O_2 saturation levels may differ substantially under ischemic conditions. Yet another confounding factor is the different Hb oxygenation in arteries versus veins. For these reasons, oxygenation as provided by NIRSI is an average value that includes contributions from cellular Mb and arterial, venous, and capillary Hb.

While the spectral features of Mb are shifted from those of Hb by a few nanometers, in principle permitting separate measurements of Mb and Hb oxygenation,[25,26,28] the coarse spectral resolution and data point spacing (10 nm) employed in this study precludes such discrimination. This does not preclude achieving the central aim of this work however, which is to provide a completely noninvasive imaging tool to assess and quantify overall tissue (Hb+Mb) oxygenation noninva-sively with good spatial resolution and without the need for fluorochromes or contact of any apparatus with the tissue.

Although the penetration of the near-infrared light into cardiac tissue is much deeper than that for visible light, it is limited to 5 to 10 mm of the subepicardial and adjacent midmural layers; oxygenation of the subendocardial and adjacent midmural tissue cannot be assessed by this method. Despite the lack of significant transmural flow gradient in pig hearts *in vivo* both under normal and ischemic conditions,[51–54] oxygenation of the subendocardial layers can be different from that of the subepicardium. First, flow and O_2 supply can be reduced by compression of subendocardial vessels during systole.[55–57] Second, endocardial fibers may develop higher tension and hence consume more O_2 due to more significant wall stress relative to the subepicardium.[56,57] Measurements of transmural left ventricular oxygen tension (oxygenation) performed invasively with O_2 microelectrodes and microspectrophotometry of rapidly frozen tissue samples showed some gradient from subepicardium to subendocardium in nonporcine hearts.[55–57] In pig hearts *in vivo*, the lack of transmural differences in phosphocreatine content both in normal and ischemic areas indicates similar supply (demand) and comparable oxygenation of subepi- and subendocardial tissue.[54]

How does the near-infrared technique compare to other methods that can also provide images of regional cardiac oxygenation? Intrinsic NADH fluorescence and extrinsic phosphorescent probes reveal related but distinct parameters. Intrinsic NADH fluorescence imaging ($\sim$460 nm) has been used to monitor myocardial oxygenation in crystalloid-perfused hearts. However this technique probes only to an epicardial depth of $\sim$50 μm due to strong tissue scattering of both the excitation (360 nm) and emission uv (visible) light.[45] Detection of NADH fluorescence in blood-perfused hearts is even more difficult due to the strong absorption of light by blood Hb, as well as tissue Mb and cytochromes.[44,58] There is no simple relationship between NADH fluorescence and pO_2. The steady-state concentration of mitochondrial NADH (and hence fluorescence) depends not only on the intracellular pO_2, but also on the delivery of oxidizable substrates, such as fatty acids and pyruvate (from glucose or lactate). In addition, inhibition of the respiratory chain between NADH dehydrogenase and cytochrome c oxidase, as well as uncoupling of respiration and phosphorylation, may both affect the NADH redox state (and fluorescence) at stable oxygen concentrations.

Combining NADH fluorescence with oxygenation measurements as provided by NIRSI may provide valuable information regarding the status of the respiratory chain and coupling to phosphorylation. Indeed, the complementary nature of NADH fluorescence and exogeneous phosphorescent probes of pO_2 have been recognized and exploited previously.[42] The clearest strength of NADH fluorescence in imaging cardiac tissue is the combination of good spatial and temporal resolution. These have permitted, for example, the resolution and characterization of ischemic border zones,[31,33,35,36,39] and revealed spatial heterogeneity in oxygen delivery to hypoxic and ischemic tissues.[32,34,37,38,40] It would be of interest to characterize these features by NIRSI, and in principle it may be possible to do so. By restricting the NIRSI acquisition to only a few key wavelengths (rather than the 41
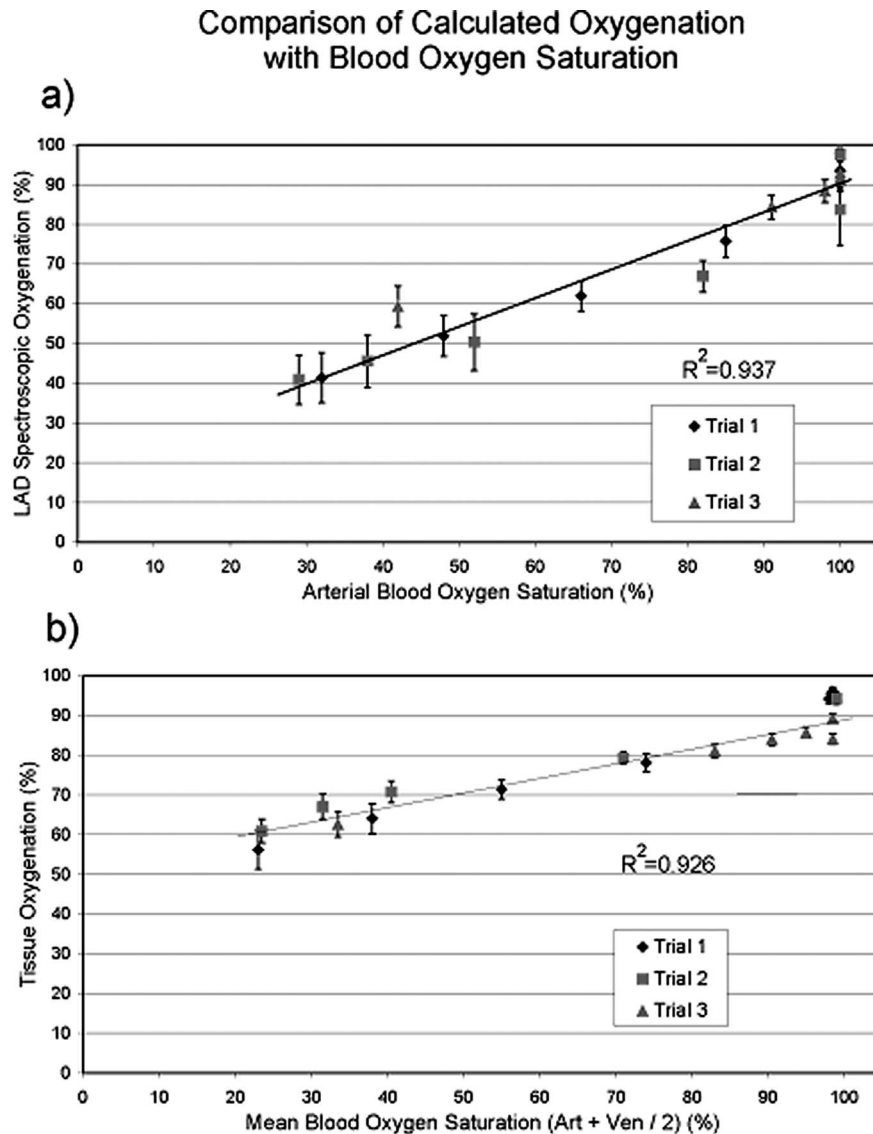
Comparison of Calculated Oxygenation with Blood Oxygen Saturation

Fig. 6 (a) Oxygenation values corresponding to the LAD artery (as determined from NIRS images) plotted against arterial blood oxygen saturation, as determined from arterial blood samples. (b) Tissue oxygenation values (NIRS imaging) are plotted against mean blood oxygen saturation values, (arterial+venous)/2, as determined from arterial and venous blood samples. Data were acquired during the stepwise hypoxia phase.

employed here to yield full spectra in the 650 to 1050 nm region), the acquisition time may in principle be reduced to seconds. A macro lens would provide the spatial resolution required to clearly delineate the heterogeneity observed within the fluorescence photographs; a 1×1-cm field of view would yield a spatial resolution of $\sim 40\ \mu$m, which would be more than adequate for this task.

4.2 Accuracy of Derived Parameters

Fitting of the deoxy-(Hb+Mb) and oxy-(Hb+Mb) absorptivity spectra to the experimental spectra relied on a number of assumptions. The reliability of the derived oxygenation parameters may therefore be gauged by examining the nature of these assumptions and their potential impact.

The experimental spectra were assumed to be suitable for reconstruction as linear combinations of the pure absorptivity spectra of deoxy-(Hb+Mb) and oxy-(Hb+Mb) (the fitting coefficients being the product of respective concentrations and the effective path length). While this assumes uniformity of the effective optical path length, it has been previously demonstrated that fitting the spectra over a restricted spectral range (650 to 890 nm) and calculating the ratio of oxy-(Hb+Mb) to total-(Hb+Mb) (both of which are proportional to the path length) minimizes the effects of variability in path length.[46]

Comparison of the measured spectra to the absorptivity spectra of Hb or Mb and water (975-nm band) confirmed that these chromophores were the major influences governing the appearance of acquired spectra (Fig. 2). However, the weak absorptions of water at 750 and 820 nm were not included in the 650 to 890-nm spectral reconstructions and this omission may have contributed some error to the calculated oxygenation values. Overlap of these weak absorptions with those of deoxy-(Hb+Mb) and oxy-(Hb+Mb) may be partially re-

sponsible for the fact that derived oxygenation values never reached zero, even during complete ischemia. In addition, oxygen diffusion from the surrounding air through the epicardial surface could shift the balance toward higher tissue pO_2. This effect would likely be minimal, however; oxygen diffusion into the cardiac tissue does not exceed 50 μm in depth,[11] while the penetration depth of near-infrared light into the muscle tissue is much greater.[59]

Major motion artifacts due to cardiac contraction were minimized by gating image acquisition, and it was previously demonstrated that an exposure time of 80 ms produced a good signal-to-noise ratio while minimizing any apparent blurring due to motion.[46] Finally, while variability in the camera shutter speed, CCD detector sensitivity, and filter transmission characteristics may in principle contribute small amounts of noise to spectra from which the images are derived, these influences are likely negligible in practice.

5 Conclusion

NIRSI provides the means to detect changes in blood and tissue oxygenation in beating hearts that result from reductions in coronary flow by as little as 50%. Moreover, oxygenation maps derived for 50, 20, and 0% LAD flow showed progressive and significant differences, suggesting that NIRSI cannot only reveal areas of ischemia but also assess the severity without the need for either invasive probes or contrast agents. Images acquired during varying degrees of global hypoxia also demonstrated a linear relationship between spectroscopically derived oxygenation values and blood oxygen saturation values, providing a basis for quantitative, intraoperative assessment of cardiac ischemia.

References

1. G. M. Pohost, M. J. Henzlova, R. Okada, C. A. Boucher, and R. C. Bourge, "Radionuclide methods to assess cardiac perfusion, function, viability and necrosis," in *The Heart and Cardiovascular System*, H. A. Fozzard, E. Haber, R. B. Jennings, A. M. Katz, and H. E. Morgan, Eds, pp. 669–691, Raven, New York (1992).
2. J. Rodenwaldt, "Multislice computed tomography of the coronary arteries," *Eur. Radiol.* **13**, 748–757 (2003).
3. O. Muhling, M. Jerosch Herold, M. Nabauer, and N. Wilke, "Assessment of ischemic heart disease using magnetic resonance first-pass perfusion imaging," *Herz* **28**, 82–89 (2003).
4. S. A. Marshall, R. A. Levine, and A. F. Weyman, "Echocardiography in cardiac research," in *The Heart and Cardiovascular System*, H. A. Fozzard, E. Haber, R. B. Jennings, A. M. Katz, and H. E. Morgan, Eds, pp. 745–837, Raven, New York (1992).
5. H. T. Dodge and F. H. Sheehan, "Quantitative angiographic techniques," in *The Heart and Cardiovascular System*, H. A. Fozzard, E. Haber, R. B. Jennings, A. M. Katz, and H. E. Morgan, Eds, pp. 725–744, Raven, New York (1992).
6. M. Tamura, N. Oshino, and B. Chance, "A new spectroscopic approach to cardiac energy metabolism," *Recent Adv. Stud. Cardiac Struct. Metab.* **11**, 307–312 (1976).
7. M. Tamura, N. Oshino, B. Chance, and I. A. Silver, "Optical measurements of intracellular oxygen concentration of rat heart in vitro," *Arch. Biochem. Biophys.* **191**, 8–22 (1978).
8. J. H. van Beek, M. D. Osbakken, and B. Chance, "Measurement of the oxygenation status of the isolated perfused rat heart using near infrared detection," *Adv. Exp. Med. Biol.* **388**, 147–154 (1996).
9. R. Araki, M. Tamura, and I. Yamazaki, "The effect of intracellular oxygen concentration on lactate release, pyridine nucleotide reduction, and respiration rate in the rat cardiac tissue," *Circ. Res.* **53**, 448–455 (1983).
10. M. Tamura, A. Seiyama, and O. Hazeki, "Spectroscopic characteristics of rat skeletal and cardiac tissues in the visible and near-infrared region," *Adv. Exp. Med. Biol.* **215**, 297–300 (1987).
11. A. E. Arai, C. E. Kasserra, P. R. Territo, A. H. Gandjbakhche, and R. S. Balaban, "Myocardial oxygenation in vivo: optical spectroscopy of cytoplasmic myoglobin and mitochondrial cytochromes," *Am. J. Physiol.* **277**, H683–H697 (1999).
12. F. W. Heineman, V. V. Kupriyanov, R. Marshall, T. A. Fralix, and R. S. Balaban, "Myocardial oxygenation in the isolated working rabbit heart as a function of work," *Am. J. Physiol.* **262**, H255–H267 (1992).
13. V. V. Kupriyanov, R. A. Shaw, B. Xiang, H. Mantsch, and R. Deslauriers, "Oxygen regulation of energy metabolism in isolated pig hearts: a near-IR spectroscopy study," *J. Mol. Cell. Cardiol.* **29**, 2431–2439 (1997).
14. J. R. Williamson and T. L. Rich, "Mitochondrial function in normal and hypoxic states of the myocardium," *Adv. Myocardiol* **4**, 271–285 (1983).
15. B. de Groot, C. J. Zuurbier, and J. H. van Beek, "Dynamics of tissue oxygenation in isolated rabbit heart as measured with near-infrared spectroscopy," *Am. J. Physiol.* **276**, H1616–H1624 (1999).
16. H. Kanaide, R. Yoshimura, N. Makino, and M. Nakamura, "Regional myocardial function and metabolism during acute coronary artery occlusion," *Am. J. Physiol.* **242**, H980–H989 (1982).
17. N. Makino, H. Kanaide, R. Yoshimura, and M. Nakamura, "Myoglobin oxygenation remains constant during the cardiac cycle," *Am. J. Physiol.* **245**, H237–H243 (1983).
18. W. J. Parsons, J. C. Rembert, R. P. Bauman, J. C. Greenfield Jr., and C. A. Piantadosi, "Dynamic mechanisms of cardiac oxygenation during brief ischemia and reperfusion," *Am. J. Physiol.* **259**, H1477–H1485 (1990).
19. W. J. Parsons, J. C. Rembert, R. P. Bauman, F. G. Duhaylongsod, J. C. Greenfield Jr., and C. A. Piantadosi, "Myocardial oxygenation in dogs during partial and complete coronary artery occlusion," *Circ. Res.* **73**, 458–464 (1993).
20. M. Kawasuji, T. Yasuda, S. Tomita, N. Sakakibara, H. Takemura, and Y. Watanabe, "Near-infrared monitoring of myocardial oxygenation during intermittent warm blood cardioplegia," *Eur. J. Cardiothorac. Surg.* **12**, 236–241 (1997).
21. M. Kawasuji, S. Tomita, T. Yasuda, N. Sakakibara, H. Takemura, and Y. Watanabe, "Myocardial oxygenation during terminal warm blood cardioplegia," *Ann. Thorac. Surg.* **65**, 1260–1264 (1998).
22. M. Kawasuji, M. Ikeda, N. Sakakibara, S. Fujii, S. Tomita, and Y. Watanabe, "Near-infrared monitoring of myocardial oxygenation during ischemic preconditioning," *Ann. Thorac. Surg.* **69**, 1806–1810 (2000).
23. M. S. Thorniley, A. Lahiri, B. Glenville, C. Shurey, G. Baker, U. Ravel, J. Crawley, and C. J. Green, "Non-invasive measurement of cardiac oxygenation and haemodynamics during transient episodes of coronary artery occlusion and reperfusion in the pig," *Clin. Sci.* **91**, 51–58 (1996).
24. M. J. Perko and H. Bay-Nielsen, "Regional myocardial oxygenation during surgical revascularisation," *Cardiovasc. Surg.* **10**, 590–594 (2002).
25. K. A. Schenkman, D. R. Marble, E. O. Fiegl, and D. H. Burns, "Near-infrared spectroscopic measurement of myoglobin oxygen saturation in the presence of hemoglobin using partial least-squares analysis," *Appl. Spectrosc.* **53**, 325–331 (1999).
26. K. A. Schenkman, D. R. Marble, D. H. Burns, and E. O. Fiegl, "Optical spectroscopic method for in vivo measurement of cardiac myoglobin oxygen saturation," *Appl. Spectrosc.* **53**, 332–338 (1999).

27. K. A. Schenkman and S. Yan, "Propofol impairment of mitochondrial respiration in isolated perfused guinea pig hearts determined by reflectance spectroscopy," *Crit. Care Med.* **28**, 172–177 (2000).

28. K. A. Schenkman and W. A. Ciesielski, "Improved myoglobin saturation measurement made by partial least-squares analysis of optical reflectance spectra," *Appl. Spectrosc.* **56**, 1215–1221 (2002).

29. K. A. Schenkman, D. A. Beard, W. A. Ciesielski, and E. O. Feigl, "Comparison of buffer and red blood cell perfusion of guinea pig heart oxygenation," *Am. J. Physiol. Heart Circ. Physiol.* **285**, H1819–H18125 (2003).

30. D. J. Marcinek, W. A. Ciesielski, K. E. Conley, and K. A. Schenkman, "Oxygen regulation and limitation to cellular respiration in mouse skeletal muscle *in vivo*," *Am. J. Physiol. Heart Circ. Physiol.* **285**, H1900–H1908 (2003).

31. C. H. Barlow and B. Chance, "Ischemic areas in perfused rat hearts: measurement by NADH fluorescence photography," *Science* **193**, 909–910 (1976).

32. C. Steenbergen, G. Deleeuw, C. Barlow, B. Chance, and J. R. Williamson, "Heterogeneity of the hypoxic state in perfused rat heart," *Circ. Res.* **41**, 606–615 (1977).

33. C. H. Barlow, A. H. Harken, and B. Chance, "Evaluation of cardiac ischemia by NADH fluorescence photography," *Ann. Surg.* **186**, 737–740 (1977).

34. B. Chance, C. H. Barlow, J. Haselgrove, Y. Nakase, B. Quistroff, F. Matschinsky, and A. Mayevsky, "Microheterogeneities of redox states of perfused and intact organs," in *Microenvironments and Metabolic Compartmentation*, P. A. Srere and R. W. Estabrook, Eds., pp. 131–148, Academic Press, New York (1978).

35. W. R. Harden, C. H. Barlow, M. B. Simson, C. H. Barlow, R. Soriano, and A. H. Harken, "Display of epicardial ischemia by reduced nicotamide adenine dinucleotide fluorescence photography, electron microscopy, and ST segment mapping," *Surgery (St. Louis)* **83**, 732–740 (1978).

36. C. H. Barlow, A. H. Harken, M. B. Simson, W. Harden, H. Rastegar, and B. Chance, "Resolution of ischemic borderzone by NADH fluorophotography in isolated perfused rabbit hearts," in *Frontiers of Biological Energetics: From Electrons to Tissues*, P. L. Dutton, J. S. Leigh, and A. Scarpa, Eds., pp. 1533–1540, Academic Press, New York (1978).

37. C. Steenbergen and J. R. Williamson, "Heterogeneous coronary perfusion during myocardial hypoxia," in *Advances in Myocardiology*, M. Tajuddin, B. Bhatia, H. H. Siddiqui, and G. Rona, Eds., Vol. **2**, pp. 271–284, University Park Press, Baltimore, MD (1980).

38. J. R. Williamson, K. N. Davis and G. Medina-Ramirez, "Quantitative analysis of heterogenous NADH fluorescence in perfused rat hearts during hypoxia and ischemia," *J. Mol. Cell. Cardiol.* **14**(Suppl. 3), 29–35 (1982).

39. A. H. Harken, C. H. Barlow, W. R. Harden III, and B. Chance, "Two and three dimensional display of myocardial ischemic 'border zone' in dogs," *Am. J. Cardiol.* **42**, 954–995 (1978).

40. Ó. G. Björnsson, K. Kobayashi, and J. R. Williamson, "Inducers of adenylate cyclase reverse the effect of leukotriene D4 in isolated working guinea pig heart," *Am. J. Physiol.* **252**, H1235–H1242 (1987).

41. L. Wetstein, H. Rastegar, C. H. Barlow, and A. H. Harken, "Delineation of myocardial ischemia in an isolated blood-perfused rabbit heart preparation," *J. Med. Chem.* **37**, 285–289 (1984).

42. C. H. Barlow, D. A. Rorvik, and J. J. Kelly, "Imaging epicardial oxygen," *Ann. Biomed. Eng.* **26**, 76–85 (1998).

43. W. L. Rumsey, J. M. Vanderkooi, and D. F. Wilson, "Imaging of phosphorescence: a novel method for measuring oxygen distribution in perfused tissue," *Science* **241**, 1649–1651 (1988).

44. W. L. Rumsey, M. Pawlowski, N. Lejavardi, and D. F. Wilson, "Oxygen pressure distribution in the heart *in vivo* and evaluation of the ischemic 'border zone'," *Am. J. Physiol.* **266**, H1676–H1680 (1994).

45. S. P. Nighswander-Rempel, R. A. Shaw, J. R. Mansfield, M. Hewko, V. V. Kupriyanov, and H. H. Mantsch, "Regional variations in myocardial tissue oxygenation mapped by near-infrared spectroscopic imaging," *J. Mol. Cell. Cardiol.* **34**, 1195–1203 (2002).

46. S. P. Nighswander-Rempel, R. A. Shaw, V. V. Kupriyanov, J. Rendell, B. Xiang, and H. H. Mantsch, "Mapping tissue oxygenation in the beating heart with near-infrared spectroscopic imaging," *Vib. Spectrosc.* **32**, 85–94 (2003).

47. V. V. Kupriyanov, S. P. Nighswander-Rempel, and B. Xiang, "Mapping regional oxygenation and flow in pig hearts *in vivo* using near-infrared spectroscopic imaging," *J. Mol. Cell. Cardiol.* **37**, 947–957 (2004).

48. S. P. Nighswander-Rempel, V. V. Kupriyanov, and R. A. Shaw, "Relative contributions of hemoglobin and myoglobin to near-infrared spectroscopic images of cardiac tissue," *Appl. Spectrosc.* **59**, 190–193 (2005).

49. V. V. Kupriyanov, B. Xiang, K. W. Butler, M. St. Jean, and R. Deslauriers, "Energy metabolism, intracellular Na+ and contractile function in isolated pig and rat hearts during cardioplegic ischemia and reperfusion: 23Na- and 31P-NMR studies," *Basic Res. Cardiol.* **90**, 220–233 (1995).

50. B. A. Wittenberg and J. B. Wittenberg, "Transport of oxygen in muscle," *Annu. Rev. Physiol.* **51**, 857–878 (1989).

51. A. S. Most, D. O. Williams, and R. W. Millard, "Acute coronary occlusion in the pig: effect of nitroglycerin on regional myocardial blood flow," *Am. J. Cardiol.* **42**, 947–953 (1978).

52. D. C. Warltier, M. G. Zyvoloski, G. J. Gross, and H. L. Brooks, "Subendocardial versus transmural myocardial infarction: relationship to the collateral circulation in canine and porcine hearts," *Can. J. Physiol. Pharmacol.* **60**, 1700–1706 (1982).

53. R. E. Patterson and E. S. Kirk, "Analysis of coronary collateral structure, function, and ischemic border zones in pigs," *Am. J. Physiol.* **244**, H23–H31 (1983).

54. W. Schaper, K. Binz, S. Sass, and B. Winkler, "Influence of collateral blood flow and of variations in MVO2 on tissue-ATP content in ischemic and infarcted myocardium," *J. Mol. Cell. Cardiol.* **19**, 19–37 (1987).

55. E. O. Feigl, "Coronary physiology," *Physiol. Rev.* **63**, 1–205 (1983).

56. R. A. Olsson and W. J. Bugni, "Coronary circulation," in *The Heart and Cardiovascular System*, H. A. Fozzard, E. Haber, R. B. Jennings, A. M. Katz, and H. E. Morgan, Eds., pp. 987–1037, Raven, New York (1986).

57. J. A. E. Spaan and P. A. Wieringa, "Oxygen exchange between blood and tissue in the myocardium," in *Coronary Blood Flow: Mechanics, Distribution and Control*, J. A. E. Spaan, Eds., pp. 291–332, Kluwer, Dordrecht, The Netherlands (1991).

58. J. M. Coremans, C. Ince, H. A. Bruining, and G. J. Puppels, "(Semi-)quantitative analysis of reduced nicotinamide adenine dinucleotide fluorescence images of blood-perfused rat heart," *Biophys. J.* **72**, 1849–1860 (1997).

59. F. F. Jöbsis, "Noninvasive, infrared monitoring of cerebral and myocardial oxygen sufficiency and circulatory parameters," *Science* **198**, 1264–1267 (1977).